energies

MDPI

Article

Adaptive Damping Design of PMSG Integrated Power System with Virtual Synchronous Generator Control

Jun Deng [1], Jianbo Wang [1], Shupeng Li [1], Haijing Zhang [1,*], Shutao Peng [1] and Tong Wang [2,*]

[1] State Grid Shaanxi Electric Power Research Institute, Xi'an 710100, China; d.jone@163.com (J.D.); 15389083826@163.com (J.W.); 13689296785@163.com (S.L.); newpking@126.com (S.P.)

[2] School of Electrical & Electronic Engineering, North China Electric Power University, Changping District, Beijing 102206, China; hdwangtong@ncepu.edu.cn

* Correspondence: zh_hj@126.com (H.Z.); hdwangtong@ncepu.edu.cn (T.W.); Tel.: +86-2989698550 (H.Z.); +86-1061771407(T.W.)

Received: 19 March 2020; Accepted: 16 April 2020; Published: 19 April 2020



Abstract: With the continuous development of wind power capacity, a large number of wind turbines connected by power electronic devices make the system inertia lower, which leads to the problem of system frequency stability degradation. The virtual synchronous generator (VSG) control can make wind turbines possess inertia and damping. However, the stochastic dynamic behavior of wind generation results in the stochastic changing of operating condition; this paper presents an adaptive subsynchronous oscillation (SSO) damping control method for the wind generation with VSG control. Firstly, the small signal model of the permanent magnet synchronous generator (PMSG) with VSG is built, and the model of state space is derived and built. The active power of PMSG is selected as the variable parameter vector to establish a polytopic linear variable parameter system model. Then, based on the hybrid H_2/H_∞ control method, each vertex state feedback matrix is solved by linear matrix inequality, and a subsynchronous oscillation adaptive damping controller with polytope is obtained. Finally, the 4-machine 2-area system connected to two PMSGs with VSG control is used as the test system for time domain simulation. The simulation results demonstrate that the LPV based adaptive damping controller could provide enough damping under the circumstances of wider changes of wind power outputs.

Keywords: virtual synchronous generator; adaptive damping control; PMSG; LPV

1. Introduction

Resources shortages in the world are becoming more dominant, and the development of renewable energy generation technologies is extremely serious. In recent years, wind power generation has become one of the most fast-growing clean energy sources in China, and the installed capacity is increasing rapidly [1,2]. The stochastic volatility of primary energy, such as wind energy, determines the random volatility of the wind power output. With the expansion of wind power grid integration, the randomness and volatility of the system are more severe, and the random drift of system operating points is increasingly prominent. The power system stability is facing severe changes as it is impacted by the grid connected large-scale wind power [3–5].

The low inertia due to wind power generation has been gaining a lot of attention [6–8]. When the traditional power system is in the dynamic transient process, the inertia of a synchronous generator could provide enough damping to prevent the deterioration of the power system. Hence, inertia is one of the important factors for maintaining the frequency stability and transient stability. Therefore, many scholars have proposed many means to improve the inertia of wind power generation, such as

synthetic virtual inertia and virtual synchronous generator (VSG) control. However, synthetic virtual inertia control could simulate the inertia of the synchronization generator, while the VSG control could not only simulate the inertial characteristic, but also the synchronization and damping behavior. The virtual synchronous generator technology is based on the power electronic converter in the new energy application [9,10]. The control algorithm is used to simulate the primary frequency modulation, voltage regulation and inertia and damping behavior of the synchronous generator so that it has the same steady state and electromechanical dynamics as the synchronous generator. Many experts and scholars have achieved fruitful research results in the grid adaptability, control stability and system application of virtual synchronous generator technology [11–14]. In 2016, State Grid Corporation started the demonstration application of virtual synchronous generator technology and core equipment in the power system for absorbing high-permeability new energy in the Zhangbei Fengshen Storage and Depot demonstration power station, and in the inverter for existing wind turbine and photovoltaic power generation.

The use of virtual synchronous generation control technology for wind power is the key to improving the friendliness of clean energy and is also the trend for efficient use of renewable energy. However, the VSG control allows the wind farm to take part in the power system frequency regulation for enhancing the frequency stability. In the meantime, the interaction channel between the wind power generation and power grid is opened through the active power after disturbance occurred. The impact caused by the interaction channel on the subsynchronous oscillation (SSO) could not be overlooked. The virtual synchronous machine control strategy and the converter control parameters are optimized, and the VSG damping control is added in the converter to form a damping of the oscillation of the sub-synchronous frequency band, which is beneficial to the suppression of the sub-synchronous oscillation. The design of traditional power system controllers is carried out under typical operating conditions, that is, the system component parameters, operating conditions and interference modes that have been given [15,16]. Because of the intermittent and strong random fluctuation of wind power, the random drift behavior of the operating condition of the renewable energy power system in the operating space makes the traditional controller design, based on the typical operating conditions, show the defect that the adaptability is obviously insufficient, and it is difficult to create wind power. The random drift behavior of the grid-connected system is effectively tracked, making it difficult to effectively be damped. Therefore, it is necessary to study adaptive damping control strategies that can effectively track the random drift behavior of the system.

At present, the control methods for power system operating point fluctuations mainly include H_∞ control [17], fuzzy control [18], structural singular value method [19] and so on. However, these methods generally fluctuate slightly for system parameters. In the case of the operating condition of the wind power system changes within a wider range, the damping effect of the controller may not be guaranteed. Recently, due to continuous development of robust control, the variable gain theory based on the linear parameter varying (LPV) system is applied in the field of power system control [20] to coordinate the power system stabilizers.

In this paper, the variable-gain theory based on the linear variable parameter system is used to effectively track the random drift behavior of the wind integrated system, so as to realize the adaptive damping control strategy. Firstly, the dynamic model of the PMSG integrated power system is built, including the dynamic models of PMSG and VSG, and then the linearized state space model is derived. Secondly, the polytopic LPV model of wind power system is established, and the state feedback matrix is solved for each vertex by hybrid H_2/H_∞ control. Finally, an adaptive damping controller is obtained based on the feedback matrix design of each vertex. The test systems adopt the 11-bus system and 39-bus system with PMSGs added. The simulation results demonstrate that the proposed SSO control by employing a polytopic LPV system can effectively suppress the SSO mode in the case of the fluctuating wind output.

2. Dynamic Model of PMSG Integrated Power Systems

2.1. Mathematical Model of PMSG

The permanent magnet synchronous generator (PMSG) is shown in Figure 1. It is composed of the asynchronous generator, a rotor-side converter, the converter controller, a grid-side converter and the converter controller.

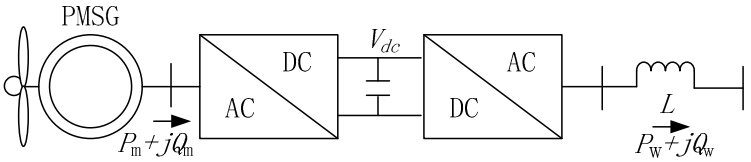


Figure 1. Permanent magnet synchronous generator structure diagram.

The dynamic model of PMSG is:

$$\begin{aligned} L_d \frac{dI_{sd}}{dt} &= \omega L_q I_{sq} - R_s I_{sd} - U_{sd} \\ L_q \frac{dI_{sq}}{dt} &= -\omega L_d I_{sd} - R_s I_{sq} - U_{sq} + \omega \Psi_f \end{aligned} \tag{1}$$

where I_{sd} represents the d-axis component of the stator winding current, and I_{sq} represents the q-axis component of the stator winding current. U_{sd} and U_{sq} represent the d-axis and q-axis components of the rotor winding voltage, respectively; ω is the electric angular speed of generator; L_d and L_q represent the d-axis and q-axis components of the stator inductance; Ψ_f is the rotor permanent magnet flux.

The rotor motion equation of PMSG based on the single mass model is as follows:

$$\frac{J_w}{np}\frac{d\omega}{dt} = T_w - T_e - D(\omega - \omega_0) \tag{2}$$

where D represents the damping coefficient; J_w denotes the motor inertia time constant; T_w and T_e represent the mechanical torque and electromagnetic torque of generator rotor, respectively; np represent the number of pole pairs; ω_0 is the rotor speed reference value.

The differential equation model of the intermediate capacitor is the expression in Equation (3).

$$\frac{dV_{dc}}{dt} = \frac{P_s + P_g}{C_{dc} V_{dc}} \tag{3}$$

where C_{dc} represents the capacitance value of the capacitor; V_{dc} represent the voltage of the capacitor; P_s represents the active power injected from the rotor-side converter to the capacitor; P_g represents the active power injected to the grid side converter.

The filter inductance between the grid-side converter and the grid is L, and its mathematical model, is as shown in Equation (4).

$$\begin{aligned} L\frac{dI_{gd}}{dt} &= U_{gd} - U_{cd} + \omega L I_{gq} \\ L\frac{dI_{gq}}{dt} &= U_{gq} - U_{cq} - \omega L I_{gd} \end{aligned} \tag{4}$$

where I_{gd} and I_{gq} represent the d-axis and q-axis components of the AC side current; U_{cd} and U_{cq} are the d and q components of the AC side voltage of the grid-side converter in d-q coordinates; U_{gd} and U_{gq} represent the d and q components of the grid-side voltage in d-q coordinates, respectively.

The intermediate variables of the outer loop of speed x_1, the inner loop of the stator current q-axis component x_2 and the inner loop of the stator current d-axis component x_3 are introduced

in the rotor-side converter control system, respectively, and the dynamic equation can be described as follows:

$$\begin{cases} \frac{dx_1}{dt} = K_{i1}(\omega - \omega_{ref}) \\ \frac{dx_2}{dt} = K_{i2}(I_{sqref} - I_{sq}) \\ \frac{dx_3}{dt} = K_{i3}(I_{sqref} - I_{sd}) \end{cases} \tag{5}$$

where K_{i1}, K_{i2} and K_{i3} represent the integral coefficients of the relative PI loops. I_{sqref} and I_{sqref} are the control reference values of the d-axis and q-axis currents of the stator windings, respectively. The control diagram of the machine-side converter is shown in Figure 2.

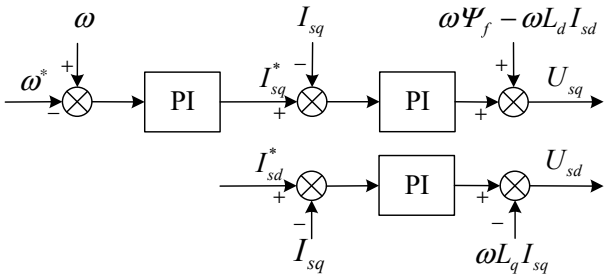


Figure 2. Control diagram of machine-side converter.

The intermediate variables of the DC voltage outer loop x_4, current q-axis inner loop x_5, reactive power outer loop x_6 and current d-axis inner loop x_7 of grid-side converter control system are introduced, respectively, and the dynamic equation of the grid-side converter controller of PMSG can be described as follows:

$$\begin{cases} \frac{dx_4}{dt} = K_{i4}(V_{dc} - V_{dcref}) \\ \frac{dx_5}{dt} = K_{i5}(I_{gdref} - I_{gd}) \\ \frac{dx_6}{dt} = K_{i6}(Q_w - Q_{wref}) \\ \frac{dx_7}{dt} = K_{i7}(I_{gqref} - I_{gq}) \end{cases} \tag{6}$$

where K_{i4}, K_{i5}, K_{i6} and K_{i7} are the integral coefficients of the relative PI loops; Q_{wref} represents the referred reactive power control of grid-side converter; I_{gdref} and I_{gdref} represent the reference value of the d and q-axis current control of grid-side converter, respectively; V_{dcref} represents the reference value of DC capacitor voltage control. The control diagram of the machine-side converter is shown in Figure 3.

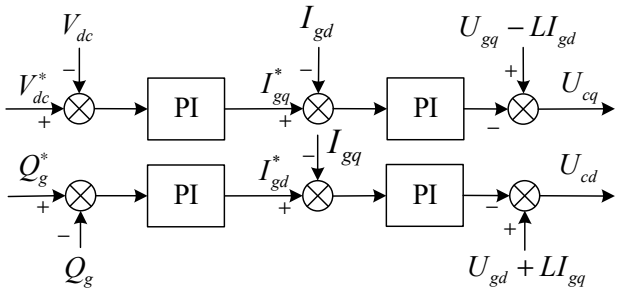


Figure 3. Control diagram of grid-side converter.

2.2. Dynamic Model of VSG Control

The equations of the VSG control model are shown in Figure 4. The dynamic model of VSG is shown in Equation (7), where *Dmp* is the damping coefficient of VSG, and J_m is the inertia of VSG.

K_m is the gain of the reactive power controller. The outputs of the Pulse width modulation (PWM) generation are sent as the input of the PWM of converter of PMSG.

$$\begin{cases} \omega_g = \frac{1}{J_m s + Dmp}(P_{ref} - P) \\ \theta_m = \frac{\omega_g - \omega_0}{s} \\ V_f = \frac{K_m}{s}(Q_{ref} - Q) \end{cases} \tag{7}$$

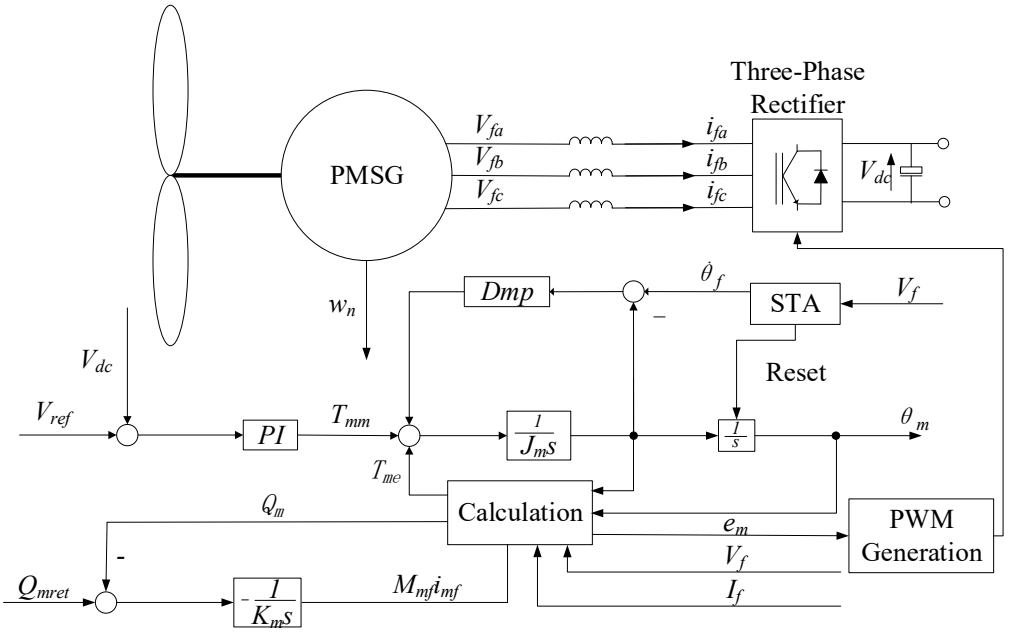


Figure 4. PMSG with virtual synchronous generator (VSG) control structure diagram.

2.3. The Linearization State Space

The PMSG dynamic model in Equations (1)–(7) is linearized to gain the small signal model of MPSG with VSG control.

$$\begin{aligned} \frac{d\Delta \boldsymbol{X}_W}{dt} &= \boldsymbol{A}_W \Delta \boldsymbol{X}_W + \boldsymbol{B}_W \Delta \boldsymbol{U}_W \\ \Delta \boldsymbol{I}_W &= \boldsymbol{C}_W \Delta \boldsymbol{X}_W + \boldsymbol{D}_W \Delta \boldsymbol{U}_W \end{aligned} \tag{8}$$

In Equation (6), $\Delta \boldsymbol{X}_W$ is the MPSG state variable, $\Delta \boldsymbol{U}_W = [\Delta U_d, \Delta U_q]^T$ is the MPSG bus voltage and $\Delta \boldsymbol{I}_W = [\Delta I_d, \Delta I_q]^T$ is the MPSG bus injection current.

By combining Equation (8), the linearization model of the synchronous generator's state equations and the grid network equation considering load, the linearized state space model of the whole system could be deduced as Equation (9).

$$\begin{aligned} \frac{d\Delta \boldsymbol{X}}{dt} &= \boldsymbol{A} \Delta \boldsymbol{X} + \boldsymbol{B} \Delta \boldsymbol{u} \\ \Delta \boldsymbol{y} &= \boldsymbol{C} \Delta \boldsymbol{X} + \boldsymbol{D} \Delta \boldsymbol{u} \end{aligned} \tag{9}$$

where $\Delta \boldsymbol{X} = [\Delta X_1, \Delta X_2 \cdots \Delta X_n]^T$ is the state vector, which is composed of the states of PMSG and synchronous generator; $\Delta \boldsymbol{u} = [\Delta u_1, \Delta u_2 \cdots \Delta u_r]^T$ is the input vector; $\Delta \boldsymbol{y} = [\Delta y_1, \Delta y_2 \cdots \Delta y_m]$ is the output vector.

3. LPV Based Adaptive Damping Control Scheme

Gain scheduling is a widely used technique for controlling certain classes of linear time-varying systems, and it is also effective for nonlinear systems. Instead of seeking a single robust controller for the entire operating range, gain scheduling consists of designing a series of controllers, switching controllers once the operating conditions change. LVP is a time-varying vector of physical parameters $p(t)$, which

varies with time. The following figure is a simple model of systems. During the dynamic process of the system, the parameters of the dynamic equations will vary with operating conditions. When these parameters change in a wider range, it is often impossible to create a satisfactory performance over the entire operating range with a single robust controller applied. If the parameters can be measured online, it will be beneficial to the system stability by using controllers that incorporate these measured variables to adaptively provide control performance for the current operating conditions as shown in Figure 5. Such controllers will be scheduled by the parameters that can be measured.

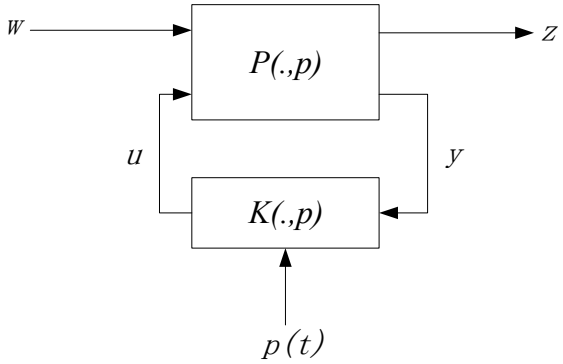


Figure 5. Gain-scheduled problem.

3.1. Polymorphic LPV System

Due to the Jacobian linearization method, the nonlinear model of the whole power system integrated wind PMSG that considers the random behavior of the operating point can be transformed into a linear variable parameter system. A linear variable parameter system refers to a system in which the state space matrix elements depend on a continuous time varying parameter vector. The variation of the parameter vector can be obtained by online measurement, and its range of variation is bounded and determinable. An LPV system for an H_2/H_∞ control model can be represented by a state space equation:

$$\begin{cases} \dot{\boldsymbol{x}}(t) = \boldsymbol{A}(\rho(t))\boldsymbol{x}(t) + \boldsymbol{B}_1(\rho(t))\boldsymbol{w}(t) + \boldsymbol{B}_2(\rho(t))\boldsymbol{u}(t) \\ \boldsymbol{z}_\infty = \boldsymbol{C}_\infty(\rho(t))\boldsymbol{x}(t) + \boldsymbol{D}_{\infty 1}(\rho(t))\boldsymbol{w}(t) + \boldsymbol{D}_{\infty 2}(\rho(t))\boldsymbol{u}(t) \\ \boldsymbol{z}_2 = \boldsymbol{C}_2(\rho(t))\boldsymbol{x}(t) + \boldsymbol{D}_{21}(\rho(t))\boldsymbol{w}(t) + \boldsymbol{D}_{22}(\rho(t))\boldsymbol{u}(t) \end{cases}, \tag{10}$$

where $\boldsymbol{x}$ is the wind power system state vector, including the synchronous generator state variable and the state variable of PMSG and VSG; $\boldsymbol{u}$ is control input vector; $\boldsymbol{w}$ is the external disturbance input vector, according to the system disturbance; z_∞ and z_2 respectively indicating the H_∞ and H_2 indicators. $\boldsymbol{A}$ represents the state matrix. $\boldsymbol{B}_1$ represent the disturbance input matrix; $\boldsymbol{B}_2$ the input matrix. $\boldsymbol{C}_\infty$,$\boldsymbol{D}_{\infty 1}$ and $\boldsymbol{D}_{\infty 2}$ represent the state variables according to the H_∞ performance index, the disturbance matrix and the control input coefficient matrix; $\boldsymbol{C}_2$, $\boldsymbol{D}_{21}$ and $\boldsymbol{D}_{22}$ are respectively related to the H_2 performance index with state variables, disturbance inputs and coefficient matrices for control inputs.

The LPV system can be represented by a polytopic shape. If there are m parameter variables in the variable parameters of the LPV system, the corresponding polymorphic LPV system has vertices $N = 2^m$, and the system variable parameters are N related vertices b_k, $k = 1, 2, \cdots, N$ of the polytopic vertices. Constantly changing, the variable parameter ρ satisfies:

$$\rho \in co(b_k, k = 1, 2, \cdots, N) = \left\{ \sum_{k=1}^{N} a_k b_k : \sum_{k=1}^{N} a_k = 1, a_k \geq 0 \right\}. \tag{11}$$

At the same time, the state space matrix of the LPV system also changes within the polymorphic matrix of N related vertices:

$$\begin{bmatrix} \boldsymbol{A}(\rho) & \boldsymbol{B}_1(\rho) & \boldsymbol{B}_2(\rho) \\ \boldsymbol{C}_\infty(\rho) & \boldsymbol{D}_{\infty 1}(\rho) & \boldsymbol{D}_{\infty 2}(\rho) \\ \boldsymbol{C}_2(\rho) & \boldsymbol{D}_{21}(\rho) & \boldsymbol{D}_{22}(\rho) \end{bmatrix} \in co\left\{ \begin{bmatrix} \boldsymbol{A}(b_k) & \boldsymbol{B}_1(b_k) & \boldsymbol{B}_2(b_k) \\ \boldsymbol{C}_\infty(b_k) & \boldsymbol{D}_{\infty 1}(b_k) & \boldsymbol{D}_{\infty 2}(b_k) \\ \boldsymbol{C}_2(b_k) & \boldsymbol{D}_{21}(b_k) & \boldsymbol{D}_{22}(b_k) \end{bmatrix}, k = 1, 2, \cdots, N \right\} \tag{12}$$

Further, using the convex decomposition technique, the convex combination of the matrix of the vertex system can be approximated by changing the coefficient α_k and the actual system matrix. The error of the convex combination of the vertex system matrix and the actual system matrix can be measured by the difference between the two matrices L_2 norm, such as that shown in Equation (13). Let α_k change from 0 to 1 with a step size of 0.01. By traversing the calculation, select γ as the lowest coefficient α_k to represent the actual system matrix. Then, the state space matrix of the polymorphic LPV system can be represented by Equation (14).

$$\gamma = \left\| \begin{bmatrix} \boldsymbol{A}(\rho) & \boldsymbol{B}_1(\rho) & \boldsymbol{B}_2(\rho) \\ \boldsymbol{C}_\infty(\rho) & \boldsymbol{D}_{\infty 1}(\rho) & \boldsymbol{D}_{\infty 2}(\rho) \\ \boldsymbol{C}_2(\rho) & \boldsymbol{D}_{21}(\rho) & \boldsymbol{D}_{22}(\rho) \end{bmatrix} - \sum_{k=1}^{N} \alpha_k \begin{bmatrix} \boldsymbol{A}(b_k) & \boldsymbol{B}_1(b_k) & \boldsymbol{B}_2(b_k) \\ \boldsymbol{C}_\infty(b_k) & \boldsymbol{D}_{\infty 1}(b_k) & \boldsymbol{D}_{\infty 2}(b_k) \\ \boldsymbol{C}_2(b_k) & \boldsymbol{D}_{21}(b_k) & \boldsymbol{D}_{22}(b_k) \end{bmatrix} \right\| \tag{13}$$

$$\begin{bmatrix} \boldsymbol{A}(\rho) & \boldsymbol{B}_1(\rho) & \boldsymbol{B}_2(\rho) \\ \boldsymbol{C}_\infty(\rho) & \boldsymbol{D}_{\infty 1}(\rho) & \boldsymbol{D}_{\infty 2}(\rho) \\ \boldsymbol{C}_2(\rho) & \boldsymbol{D}_{21}(\rho) & \boldsymbol{D}_{22}(\rho) \end{bmatrix} = \sum_{k=1}^{N} \alpha_k \begin{bmatrix} \boldsymbol{A}(b_k) & \boldsymbol{B}_1(b_k) & \boldsymbol{B}_2(b_k) \\ \boldsymbol{C}_\infty(b_k) & \boldsymbol{D}_{\infty 1}(b_k) & \boldsymbol{D}_{\infty 2}(b_k) \\ \boldsymbol{C}_2(b_k) & \boldsymbol{D}_{21}(b_k) & \boldsymbol{D}_{22}(b_k) \end{bmatrix} \tag{14}$$

3.2. Mixed H_2/H_∞ Control

When the parameter ρ is determined, the LPV system transitions to a linear time-invariant system:

$$\begin{cases} \dot{\boldsymbol{x}}(t) = \boldsymbol{A}\boldsymbol{x}(t) + \boldsymbol{B}_1\boldsymbol{w}(t) + \boldsymbol{B}_2\boldsymbol{u}(t) \\ \boldsymbol{z}_\infty = \boldsymbol{C}_\infty\boldsymbol{x}(t) + \boldsymbol{D}_{\infty 1}\boldsymbol{w}(t) + \boldsymbol{D}_{\infty 2}\boldsymbol{u}(t) \\ \boldsymbol{z}_2 = \boldsymbol{C}_2\boldsymbol{x}(t) + \boldsymbol{D}_{21}\boldsymbol{w}(t) + \boldsymbol{D}_{22}\boldsymbol{u}(t) \end{cases} \tag{15}$$

This paper uses state feedback to design the controller. Substituting the state feedback law $\boldsymbol{u} = \boldsymbol{K}\boldsymbol{x}$ into the open-loop system model in Equation (14), the closed-loop system model is obtained:

$$\begin{cases} \dot{\boldsymbol{x}}(t) = \boldsymbol{A}_c\boldsymbol{x}(t) + \boldsymbol{B}_1\boldsymbol{w}(t) \\ \boldsymbol{z}_\infty = \boldsymbol{C}_{\infty c}\boldsymbol{x}(t) + \boldsymbol{D}_{\infty 1}\boldsymbol{w}(t) \\ \boldsymbol{z}_2 = \boldsymbol{C}_{2c}\boldsymbol{x}(t) + \boldsymbol{D}_{21}\boldsymbol{w}(t) \end{cases} \tag{16}$$

where $\boldsymbol{A}_c = \boldsymbol{A} + \boldsymbol{B}_2\boldsymbol{K}$; $\boldsymbol{C}_{\infty c} = \boldsymbol{C}_\infty + \boldsymbol{D}_{\infty 2}\boldsymbol{K}$; $\boldsymbol{C}_{2c} = \boldsymbol{C}_2 + \boldsymbol{D}_2\boldsymbol{K}$.

A mixed H_2/H_∞ control damping controller requires the introduction of a state feedback matrix $\boldsymbol{K}$. The closed-loop linear time-invariant system meets the following objectives:

(1) H_∞ performance: the H_∞ norm of the transfer function from the disturbance signals $\boldsymbol{w}$ to the output variables $\boldsymbol{z}_\infty$ is defined as:

$$\|\boldsymbol{T}_{wz\infty}(s)\|_\infty = \sup_\omega \sigma_{\max}(\boldsymbol{T}_{wz\infty}(j\omega)) \tag{17}$$

It represents the peak of the largest singular value of the system's frequency response. From a time domain perspective, it is the worst-case steady-state gain for a sinusoidal input of any frequency. When $\boldsymbol{w}$ represents the disturbance signal with limited energy, it is $\|\boldsymbol{T}_{wz\infty}(s)\|_\infty < \gamma$.

(2) H_2 performance: the H_2 norm of the closed-loop transfer function from the disturbance signal $\boldsymbol{w}$ to the output variable $\boldsymbol{z}_2$ is defined as:

$$\|\boldsymbol{T}_{wz2}(s)\|_2 = \sqrt{\frac{1}{2\pi}\int_{-\infty}^{\infty} tr\left(\boldsymbol{T}_{wz2}^*(j\omega)\boldsymbol{T}_{wz2}(j\omega)\right)d\omega} \tag{18}$$

where $\boldsymbol{T}_{wz2}^*(j\omega)$ represents the conjugate transpose of $\boldsymbol{T}_{wz2}(j\omega)$; $tr(\cdot)$ is the trace of the matrix. The H_2 norm is the rms value of the outputs under white noise excitation. For a given normal number η, it is $\|\boldsymbol{T}_{wz2k}(s)\|_2 < \eta$.

(3) D region pole configuration: the poles of the closed loop system are required to be placed in a given D region:

$$D = \left\{s \in \mathbf{W} : \ \boldsymbol{L} + a\boldsymbol{M} + \bar{a}\boldsymbol{M}^T < 0\right\} \tag{19}$$

where $\boldsymbol{L} = \boldsymbol{L}^T$, and $\boldsymbol{M}$ is the given real matrix; $\mathbf{W}$ represents the complex field; a represents a complex number; $\bar{a}$ is a conjugate of a. The D region is as displayed in Figure 6. Equation (17) is $\boldsymbol{L} = \begin{bmatrix} 2l_0 & 0 & 0 \\ 0 & 0 & 0 \\ 0 & 0 & 0 \end{bmatrix}, \boldsymbol{M} = \begin{bmatrix} 1 & 0 & 0 \\ 0 & \sin\theta & -\cos\theta \\ 0 & \cos\theta & \sin\theta \end{bmatrix}$.

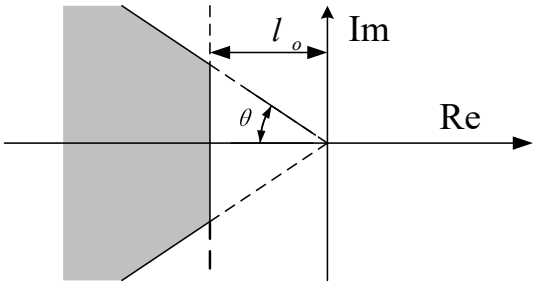


Figure 6. Regional pole configuration.

A feasible solution could be obtained by using the following linear inequalities [9] to satisfy the above constraints:

$$\begin{aligned} &\min_{\gamma,\boldsymbol{X},\boldsymbol{Y},\boldsymbol{Q}} \mu\gamma + \beta tr(\boldsymbol{Q}) \\ &\begin{bmatrix} \boldsymbol{A}\boldsymbol{X} + \boldsymbol{X}\boldsymbol{A}^T + \boldsymbol{B}_2\boldsymbol{Y} + \boldsymbol{Y}^T\boldsymbol{B}_2^T & \boldsymbol{B}_1 & \boldsymbol{X}\boldsymbol{C}_\infty^T + \boldsymbol{Y}^T\boldsymbol{D}_{\infty 2}^T \\ \boldsymbol{B}_1{}^T & -\gamma\boldsymbol{I} & \boldsymbol{D}_{\infty 1}^T \\ \boldsymbol{C}_\infty\boldsymbol{X} + \boldsymbol{D}_{\infty 2}\boldsymbol{Y} & \boldsymbol{D}_{\infty 1} & -\gamma\boldsymbol{I} \end{bmatrix} < 0 \\ &\begin{bmatrix} \boldsymbol{Q} & \boldsymbol{C}_{2k}\boldsymbol{X} + \boldsymbol{D}_{22k}\boldsymbol{Y} \\ \boldsymbol{X}\boldsymbol{C}_2{}^T + \boldsymbol{Y}^T\boldsymbol{D}_{22}^T & \boldsymbol{X} \end{bmatrix} > 0 \\ &\boldsymbol{L} \otimes \boldsymbol{X} + \boldsymbol{M} \otimes (\boldsymbol{A}\boldsymbol{X} + \boldsymbol{B}_2\boldsymbol{Y}) + \boldsymbol{M}^T \otimes (\boldsymbol{A}\boldsymbol{X} + \boldsymbol{B}_2\boldsymbol{Y})^T < 0 \\ &tr(\boldsymbol{Q}) < \eta_0{}^2 \\ &\gamma < \gamma_0 \end{aligned} \tag{20}$$

where γ_0, η_0, μ and β are the parameters given to meet different design goals; $\otimes$ represents the Kronecker product. If $(\gamma^*, \boldsymbol{X}^*, \boldsymbol{Y}^*, \boldsymbol{Q}^*)$ is the solution of the inequality, the state feedback matrix is found to be $\boldsymbol{K} = \boldsymbol{Y}^*\boldsymbol{X}^*$.

3.3. LPV-Based Gain Schedule Control

The vertices of the polymorphic LPV system are linear time-invariant systems with vertices $\begin{bmatrix} \boldsymbol{A}(b_k) & \boldsymbol{B}_1(b_k) & \boldsymbol{B}_2(b_k) \\ \boldsymbol{C}_\infty(b_k) & \boldsymbol{D}_{\infty 1}(b_k) & \boldsymbol{D}_{\infty 2}(b_k) \\ \boldsymbol{C}_2(b_k) & \boldsymbol{D}_{21}(b_k) & \boldsymbol{D}_{22}(b_k) \end{bmatrix}$, $k = 1, 2, \cdots, N$. Substituting Equation (20) can obtain a state feedback matrix of N vertices $\boldsymbol{K}_k$, $k = 1, 2, \cdots, N$. Similar to the convex decomposition structure of the LPV model, the vertex state feedback matrix $\boldsymbol{K}_k$, $k = 1, 2, \cdots, N$ is used as the N vertices of the

polymorphic LPV controller. At any position of the polytope, the idea of robust variable gain and the multi-model system convexity of LPV are used. The feature is obtained with a state feedback gain $\boldsymbol{K}$ with global characteristics:

$$\boldsymbol{K} = \sum_{k=1}^{N} \alpha_k \boldsymbol{K}_k \tag{21}$$

4. Adaptive Damping Controller Design

4.1. Test System

The four generator two area test system [21] connected to PMSGs is shown in Figure 7. The parameters of this DIFG are from reference [22]. The load is assumed to be a constant admittance in the test system. The rated active power is 100 MW. The initial active output power of both PMSGs is 0.3 p.u., and an eigenvalue analysis is performed on this system. The oscillation modes ranging below 50 Hz are shown and displayed in Table 1; the first four modes ranging from 2.5 Hz to 50 Hz are SSO modes caused by PMSGs. The damping ratios are relatively weak, which might cause the instability, and the last three modes are the low frequency modes with satisfactory damping ratios. The controller proposed in this paper mainly suppresses the SSO mode caused by PMSG. The parameters of VSG are $K_m = 2$, $Dmp = 30$, $J_m = 0.5$.

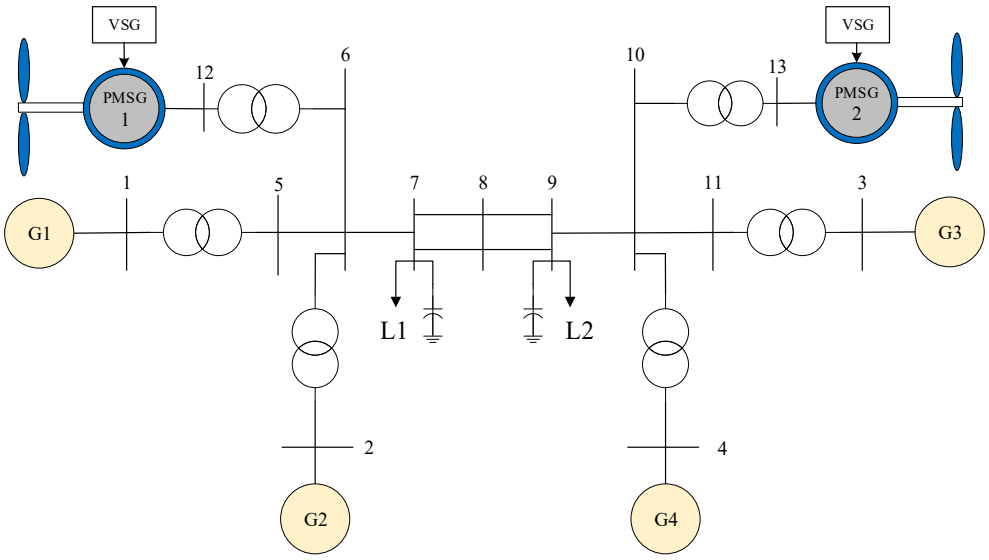


Figure 7. Modified four-generator two-area system with PMSGs.

Table 1. Eigenvalues and oscillation modes.

Mode	Eigenvalue	Freq./Hz	Damping Ratio
1	−0.3611 ± 119.7502j	19.06	0.0030
2	−0.2848 ± 107.5388j	17.12	0.0026
3	−0.1982 ± 90.3861j	14.39	0.0022
4	−0.3034 ± 74.8455j	11.91	0.0041
5	−3.9387 ± 12.8940j	2.05	0.2921
6	−4.1875 ± 11.8834j	1.89	0.3324
7	−4.0214 ± 4.5343j	0.72	0.6635

4.2. Damping Control

In this paper, a variable gain damping controller is designed by a hybrid H_2/H_∞ control based on the polytopic LPV system. We select the time-varying parameter vector $\rho(t)$ that reflects the random

drift behavior of the system operating point as the output active power of the two PMSGs. According to the operating conditions of the system, the random fluctuation range of the two PMSG active powers is 0.3 p.u. to 0.6 p.u. We establish a polytopic LPV model corresponding to the wind power system. The number of elements of the time-varying parameter vector $\rho(t)$ of the test system is 2, so the number of vertices of the polymorphic LPV system is 4. The PMSG active power of vertex 1 is 0.3 p.u.; the active power of PMSG1 in vertex 2 is 0.3 pu; the active power of PMSG2 is 0.6 pu; the active power of PMSG1 in vertex 3 is 0.6 p.u., and the active power of PMSG2 is 0.3 p.u.; the 4 PMSG active power is 0.6 p.u.

The effectiveness of the damping power oscillations depends on the operating conditions. There are two stages for the adaptive control design, including offline and online parts. In the offline stage, the controllers are designed due to different vertices. In the online stage, the controllers are combined with coefficient α_k, which changes with the output of wind generation and can be identified online. The damping controller control signal is added to the reactive power control and the active power control of the rotor side converter of the fan. Considering the H_∞ norm performance and H_2 norm performance, the hybrid H_2/H_∞ control design method is designed to minimize the performance index, which is $\mu\|T_{wz2}(s)\|_2 + \beta\|T_{wz\infty}(s)\|_\infty$. Where μ and β are the weighting factors, both take 1. We set the pole configuration area so that the SSO mode damping ratio is greater than 0.1, and the real part of the eigenvalue is less than −0.5, and we use the algorithm proposed in Section 1 to solve the state feedback matrix of the vertex. After obtaining the state feedback matrix of each vertex in the running subspace, the system adaptive damping controller can be obtained according to Equation (14). In the actual power system, the measured values of all state variables of the system are generally not available. Therefore, the state observer is designed to complete the estimation of the system state variables. The state observer follows the linearized model structure of the actual system and designs an identical system to observe the state variables.

5. Simulation and Results

5.1. 4-Generator System

In the test system, the PMSG1 active power is 0.36 p.u., and the PMSG2 active power is 0.53 p.u. as the base case, which lays inside the convex domain. If the power values change, the control performance will not be affected. The operating point parameter vector is denoted as [0.36 0.53] and the coefficient vector α is [0.04 0.76 0.2 0]. The sub-synchronous oscillation characteristic values of the system before and after the introduction of state feedback are displayed in Table 2. It can be seen that the SSO controller increases the damping ratio of the system's subsynchronous oscillation mode. The SSO mode damping ratio of the closed-loop system is greater than 0.1, and the controller meets the design requirements.

Table 2. Subsynchronous oscillation (SSO) modes of the closed-loop system.

	Frequency/Hz	**Damping Ratio**
Closed loop	20.25	0.1565
	15.43	0.1268
	12.92	0.1275
	12.79	0.1496

To further demonstrate the effectiveness of the proposed adaptive damping controller, time domain simulation is performed. At 1 s, the active reference power of each PMSG is superimposed with 5% of the disturbance, and after 0.02 s, the disturbance is cleared. Figure 8 shows the PMSG active power time domain simulation curve using the controller and not using the controller. The blue dashed line and the red solid line represent the PMSG time domain simulation curves for the

controllers not used and used, respectively. After the adaptive SSO damp controller is applied, the active power is attenuated rapidly and the system resumes stable condition at a fast speed.

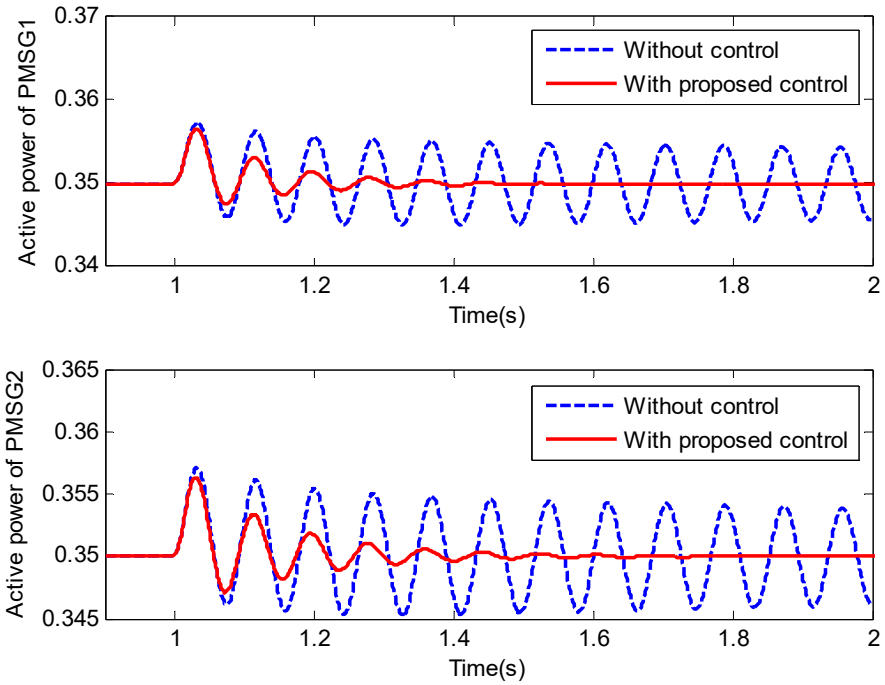


Figure 8. Active powers of PMSGs.

The adaptive controller designed in this paper is compared with the fixed parameter Hinf controller. The operating point of the Hinf controller design is the operating point of the test system when both of the PMSG active powers are 0.4 p.u., that is, the state feedback matrix is designed at vertex 1. The adaptive controller is a variable gain damping controller designed for this paper. In the test system, the initial active power of the two PMSGs is 0.4 p.u., respectively, and the controller and the parameter controller are added for time domain simulation. The time domain simulation results using different SSO damp controllers are displayed in Figure 9. The black, blue and red curves are the active powers of PMSGs without control, with Hinf control and with the proposed adaptive controller, respectively. At t = 2 s, the active power of both PMSGs becomes 0.2 p.u. When the PMSG output varies and causes the current operating condition to drift from the specific operating condition designed for the Hinf controller, then the Hinf controller will have a less effective damping effect on the subsynchronous oscillation than the adaptive controller. The adaptive damping controller based on the polytopic LPV system has a better adaptability to the random drift of the operating condition of the power system.

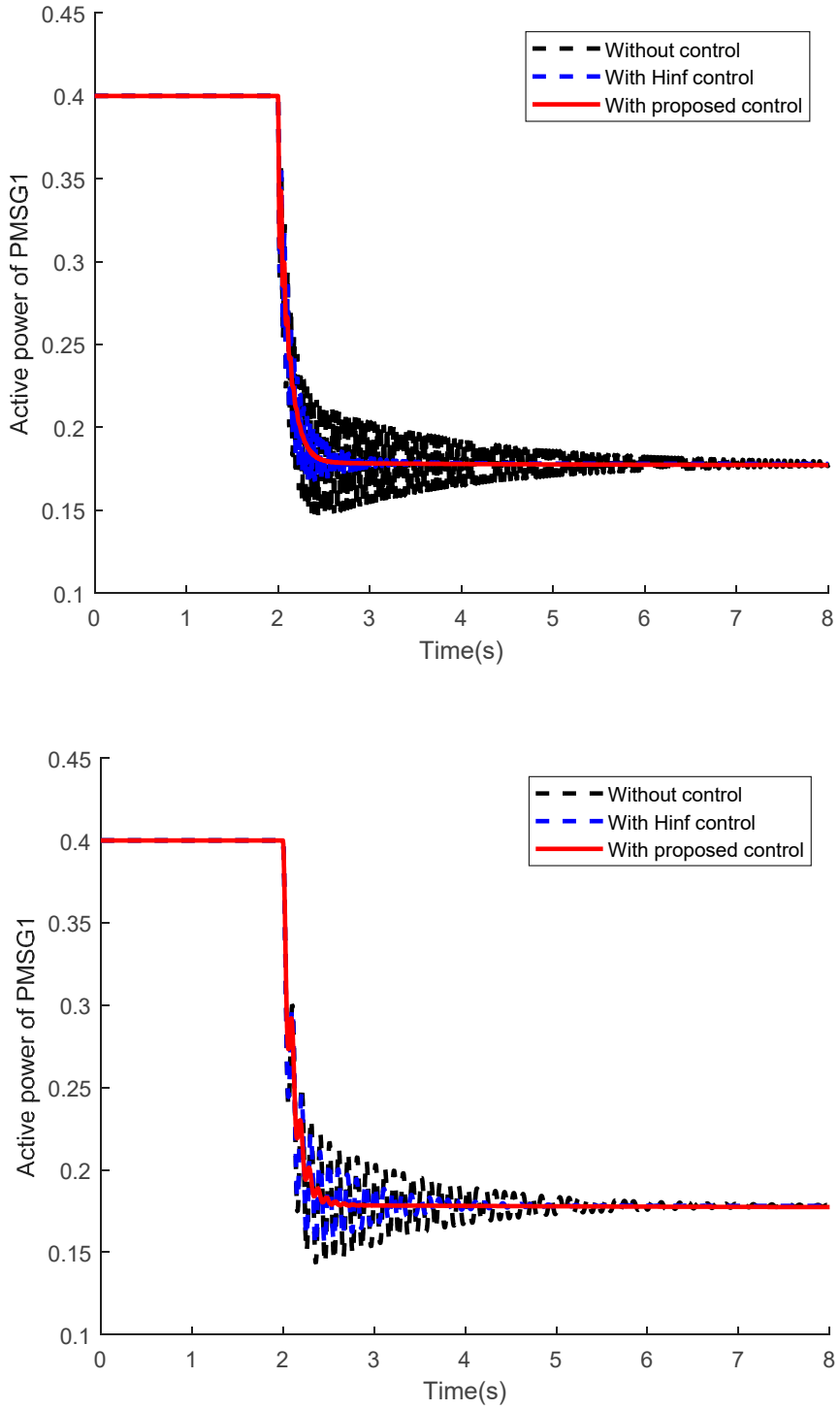


Figure 9. Active powers of PMSGs with the changing wind outputs.

5.2. 39-Bus 16-Generation Test System

The New England 39 bus system with two PMSGs as shown in Figure 10 is used as the test system to investigate the effectiveness of the proposed method further. The PMSG 1 and PMSG are added to buses 6 and 32, respectively. The SSO modes are calculated, as shown in Table 3, under the base case with the output active power of PMSG1 at 0.4 p.u., and the active power of PMSG2 at 0.4 p.u. From the table, it can be seen that there are three dominant subsynchronous oscillation modes with weak damping ratios. The number of vertices of the polymorphic LPV system is 4. The PMSGs active power

of vertex 1 are both 0.4 p.u.; the active power of PMSG1 in vertex 2 is 1.0 p.u., and the active power of PMSG2 is 0.4 p.u.; the active power of PMSG1 in vertex 3 is 0.4 p.u., and the active power of PMSG2 is 1.0 p.u. For vertex 4, the active power of the two PMSGs are both 1.0 p.u.

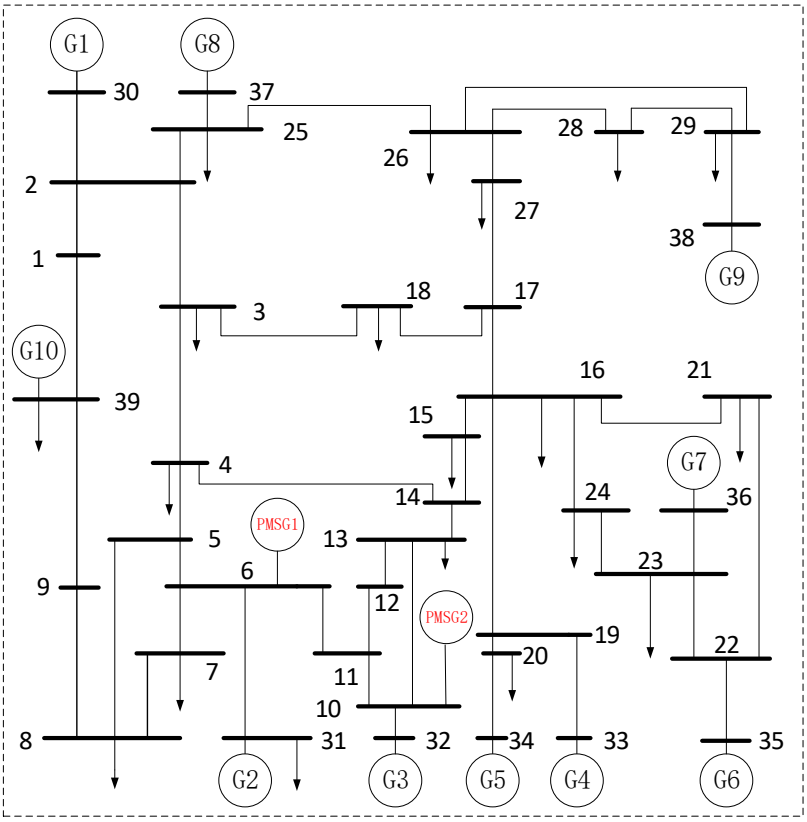


Figure 10. 39-bus system with two PMSGs added.

Table 3. Eigenvalues of SSO for open-loop system for Vertex 1.

Frequency/Hz	Damping Ratio
28.4736	0.0036
27.2591	0.0027
14.4338	0.0061

A three-phase temporary fault is set at bus 8 at t = 1 s, and then the fault clearance is set at t = 1.1 s later. The dynamic responses of the two PMSGs are shown in Figure 11. The coefficient vector α is under this situation is [0.89 0.06 0.05 0]. The blue dashed line represents the dynamic responses of PMSGs without the control from which the SSO could not mitigate. The green and red solid lines represent the dynamic responses of PMSGs with the Hinf control and with the LPV based control, respectively. By comparison with the Hinf control, the proposed control shows better performance in the case of fault.

The wind output power changes might affect the performance of controllers, and the simulation results are shown in Figure 12. The fault occurs on bus 8 at t = 1 s, and is cleared at t = 1.5 s. At t = 2 s, the wind output power of PMSG1 changes from 0.4 p.u. to 1 p. u., and at t = 4 s, the wind output power of PMSG1 changes from 0.4 p.u. to 1 p. u. The black, blue and red lines represent the dynamic responses of the active power of two PMSGs. The coefficient vector α before t = 1 s is [0.89 0.06 0.05 0]. At t = 2 s, coefficient vector α changes to [0.12 0.80 0.05 0.03] to match the operating condition, and after t = 4 s, the coefficient vector α changes to [0.02 0.12 0.11 0.75]. The simulation results as displayed

in Figure 12 demonstrate that that the proposed control could provide enough damp in the case of wind changes.

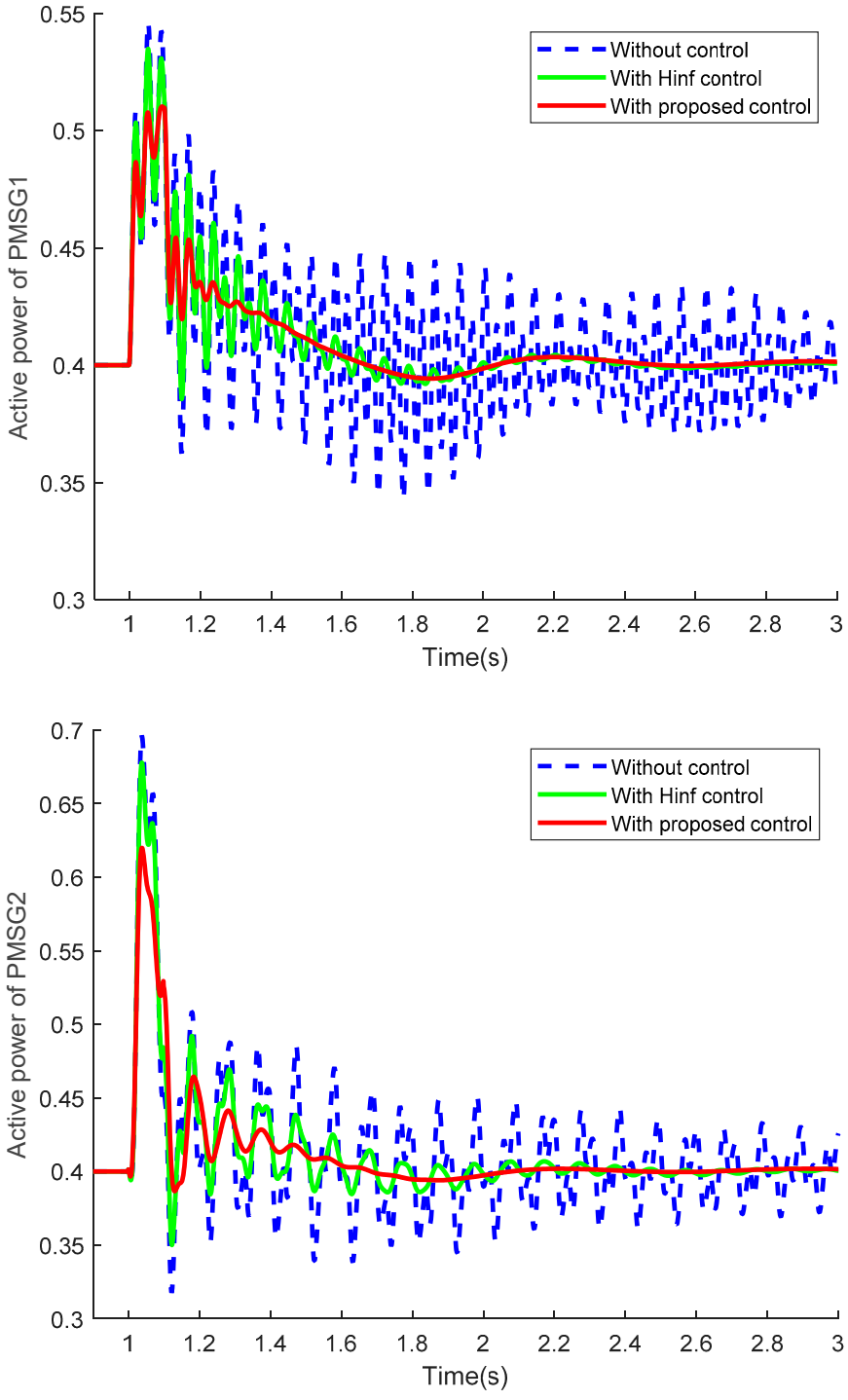


Figure 11. Active powers of PMSGs after fault.

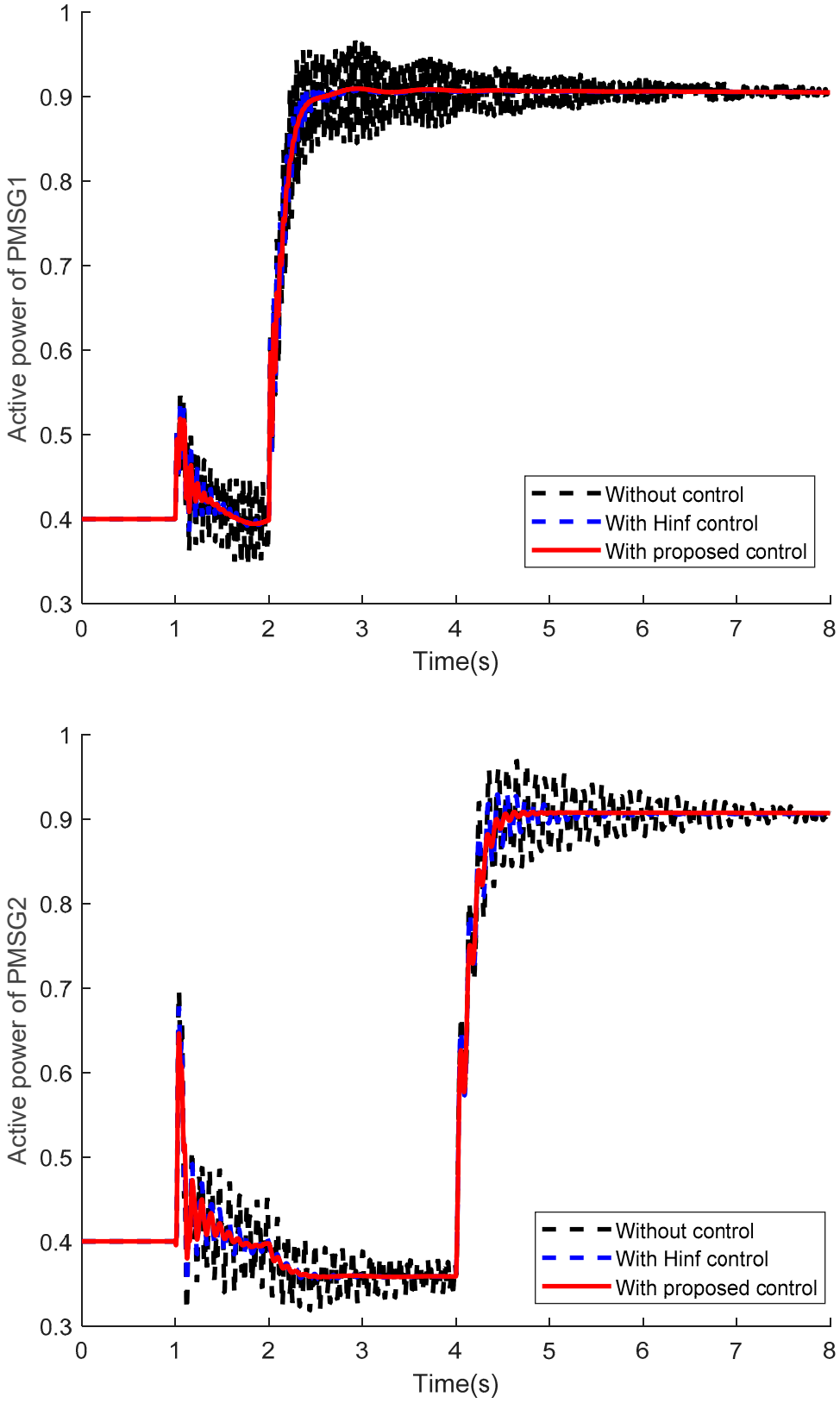


Figure 12. Active powers of PMSGs in the case of wind change.

6. Conclusions

For the PMSG integrated system with VSG control, this paper proposes a sub-synchronous oscillation adaptive damping control method. The contributions of this paper are concluded as follows:

(1) The linearized state space model of PMSG with the VSG controller is established and deduced, and the power system integrated with PMSG is also built and an eigenvalue analysis is performed.
(2) The damp controller uses a hybrid H_2/H_∞ multi-objective model to obtain the feedback signal from the VSG, thereby enhancing the damping of the power system.
(3) The polytopic LPV system model is built with the help of an H_2/H_∞ multi-objective model for the design of an adaptive controller to maintain satisfactory damping performance when the controller is randomly drifting at the operating point of the wind power system. The adaptive controller is solved by the linear matrix inequalities to obtain a feasible solution.
(4) The time domain simulation results of the four-machine two-zone system and the 39-bus system with PMSGs demonstrate that the LPV based SSO damping controller could provide enough damping in the case of wind changes.

7. Discussion

The limitation of the proposed adaptive damping is the availability of wide area signals, which are used as the feedback signals. Also, the time delay caused by the wide area feedback signals affects the control performance. Meanwhile, the central frequency controller has not been considered, but the frequency controller for maintaining the frequency stability, which gains more attention, will be the future research field of our research group.

Author Contributions: Conceptualization, J.D. and T.W.; Methodology, S.L.; Software, J.W.; Validation, H.Z. and S.P.; Formal Analysis, J.D.; Investigation, J.D.; Resources, S.L.; Data Curation, H.Z.; Writing—Original Draft Preparation, T.W.; Writing—Review & Editing, S.P.; Visualization, J.W.; Supervision, S.P.; Project Administration, T.W. All authors have read and agreed to the published version of the manuscript.

Funding: This research received no external funding.

Conflicts of Interest: The authors declare no conflict of interest.

References

1. Wang, L.; Xie, X.; Jiang, Q.; Liu, H.; Li, Y.; Liu, H. Investigation of SSR in Practical DFIG-Based Wind Farms Connected to a Series-Compensated Power System. *IEEE Trans. Power Syst.* **2015**, *30*, 2772–2779. [CrossRef]
2. Hansen, K.S.; Barthelmie, R.; Jensen, L.E.; Sommer, A. The impact of turbulence intensity and atmospheric stability on power deficits due to wind turbine wakes at Horns Rev wind farm. *Wind. Energy* **2011**, *15*, 183–196. [CrossRef]
3. Bu, S.; Chen, Z.; Xiao, L.Y.; Li, H.F.; Du, W.; Wang, H. Probabilistic Analysis of Small-Signal Stability of Large-Scale Power Systems as Affected by Penetration of Wind Generation. *IEEE Trans. Power Syst.* **2011**, *27*, 762–770. [CrossRef]
4. Wang, Z.W.; Shen, C.; Liu, F. Probabilistic Analysis of Small Signal Stability for Power Systems with High Penetration of Wind Generation. *IEEE Trans. Sustain. Energy* **2016**, *7*, 1182–1193. [CrossRef]
5. Ogura, M.; Preciado, V.M. Stability of Spreading Processes over Time-Varying Large-Scale Networks. *IEEE Trans. Netw. Sci. Eng.* **2016**, *3*, 44–57. [CrossRef]
6. Nguyen, N.; Mitra, J. An analysis of the effects and dependency of wind power penetration on system frequency regulation. *IEEE Trans. Sustain. Energy* **2016**, *7*, 354–363. [CrossRef]
7. Bevrani, H.; Ghosh, A.; Ledwich, G. Renewable energy sources and frequency regulation: Survey and new perspectives. *Renew. Power Gener.* **2010**, *4*, 438–457. [CrossRef]
8. David, N.; Wang, Z. Physical rotor inertia of DFIG wind turbines for short-term frequency regulation in low-inertia grids. In Proceedings of the 2017 IEEE Power & Energy Society General Meeting, Chicago, IL, USA, 24–27 July 2017; pp. 1–5.

9. Zhong, Q.C.; Weiss, G. Synchronverters: Inverters that mimic synchronous generators. *IEEE Trans. Ind. Electron.* **2010**, *58*, 1259–1267. [CrossRef]
10. Beck, H.P.; Hesse, R. Virtual synchronous machine. In Proceedings of the 2007 Electrical Power Quality and Utilisation, Barcelona, Spain, 9–11 October 2007; pp. 1–6.
11. Bevrani, H.T.; Miura, Y. Virtual synchronous generators: A survey and new perspectives. *Electr. Power Energy Syst.* **2014**, *54*, 244–254. [CrossRef]
12. Zhong, Q.C.; Nguyen, P.L.; Ma, Z.; Sheng, W. Self-synchronized synchronverters: Inverters without a dedicated synchronization unit. *IEEE Trans. Power Electron.* **2013**, *29*, 617–630. [CrossRef]
13. Driesen, J.; Visscher, K. Virtual synchronous generators. In Proceedings of the IEEE/PES General Meeting-Conversion Delivery of Electrical Energy in the Century, Pittsburgh, PA, USA, 20–24 July 2008; pp. 1–3.
14. Hirase, Y.; Abe, K.; Sugimoto, K.; Shindo, Y. A grid connected inverter with virtual synchronous generator model of algebraic type. *IEEJ Trans. Power Energy* **2012**, *132*, 371–380. [CrossRef]
15. Zhong, Q. Virtual Synchronous Machines: A unified interface for grid integration. *IEEE Power Electron. Mag.* **2016**, *3*, 18–27. [CrossRef]
16. Karimi-Ghartemani, M.; Iravani, M. A nonlinear adaptive filter for online signal analysis in power systems: Applications. *IEEE Trans. Power Deliv.* **2002**, *17*, 617–622. [CrossRef]
17. Singh, V.P.; Mohanty, S.R.; Kishor, N.; Ray, P.K. Robust H-infinity load frequency control in hybrid distributed generation system. *Int. J. Electr. Power Energy Syst.* **2013**, *46*, 294–305. [CrossRef]
18. Andalib, C.; Liang, X.; Zhang, H. Fuzzy-Secondary-Controller-Based Virtual Synchronous Generator Control Scheme for Interfacing Inverters of Renewable Distributed Generation in Microgrids. *IEEE Trans. Ind. Appl.* **2017**, *54*, 1047–1061. [CrossRef]
19. Liu, L.; Dong, S.; Wang, Y.; Ou, L. Clearance of flight control law based on structural singular value theory. *IEEE Trans. Aerosp. Electron. Syst.* **2015**, *51*, 2138–2147. [CrossRef]
20. Qiu, W.; Vittal, V.; Khammash, M. Decentralized power system stabilizer design using linear parameter varying approach. *IEEE Trans. Power Syst.* **2004**, *19*, 1951–1960. [CrossRef]
21. Kundur, P.; Balu, N.J.; Lauby, M.G. *Power System Stability and Control*; McGraw-hill: New York, NY, USA, 1994; Volume 7.
22. Du, W.; Bi, J.; Cao, J.; Wang, H.F. A method to examine the impact of grid connection of the DFIGs on power system electromechanical oscillation modes. *IEEE Trans. Power Syst.* **2015**, *31*, 3775–3784. [CrossRef]



© 2020 by the authors. Licensee MDPI, Basel, Switzerland. This article is an open access article distributed under the terms and conditions of the Creative Commons Attribution (CC BY) license (http://creativecommons.org/licenses/by/4.0/).